



THE UNIVERSITY *of* EDINBURGH

Edinburgh Research Explorer

Knudsen Minimum Disappearance in Molecular-Confined Flows

Citation for published version:

Corral-Casas, C, Li, J, Borg, MK & Gibelli, L 2022, 'Knudsen Minimum Disappearance in Molecular-Confined Flows', *Journal of Fluid Mechanics*, vol. 945, A28. <https://doi.org/10.1017/jfm.2022.563>

Digital Object Identifier (DOI):

[10.1017/jfm.2022.563](https://doi.org/10.1017/jfm.2022.563)

Link:

[Link to publication record in Edinburgh Research Explorer](#)

Document Version:

Peer reviewed version

Published In:

Journal of Fluid Mechanics

General rights

Copyright for the publications made accessible via the Edinburgh Research Explorer is retained by the author(s) and / or other copyright owners and it is a condition of accessing these publications that users recognise and abide by the legal requirements associated with these rights.

Take down policy

The University of Edinburgh has made every reasonable effort to ensure that Edinburgh Research Explorer content complies with UK legislation. If you believe that the public display of this file breaches copyright please contact openaccess@ed.ac.uk providing details, and we will remove access to the work immediately and investigate your claim.



Banner appropriate to article type will appear here in typeset article

1 **Knudsen Minimum Disappearance in** 2 **Molecular-Confined Flows**

3 **Carlos Corral-Casas**¹, **Jun Li**², **Matthew K. Borg**¹, and **Livio Gibelli**¹†

4 ¹Institute for Multiscale Thermofluids, School of Engineering, The University of Edinburgh, Edinburgh
5 EH9 3FB, United Kingdom

6 ²Center for Integrative Petroleum Research, College of Petroleum Engineering and Geosciences, King
7 Fahd University of Petroleum and Minerals, Dhahran 31261, Saudi Arabia

8 (Received xx; revised xx; accepted xx)

9 It is well-known that the Poiseuille mass flow rate along microchannels shows a stationary
10 point as the fluid density decreases, referred to as the Knudsen minimum. Surprisingly, if
11 the flow characteristic length is comparable to the molecular size, the Knudsen minimum
12 disappears, as reported for the first time by Wu *et al.* (*J. Fluid Mech.*, vol. 794, 2016, pp.
13 252-266). However, there is still no fundamental understanding why the mass flow rate
14 monotonically increases throughout the entire range of flow regimes. Although diffusion is
15 believed to dominate the fluid transport at the nanoscale, here we show that the Fick's first
16 law fails in capturing this behaviour, and so diffusion alone is insufficient to explain this
17 confined flow phenomenon. Rather, we show that the Knudsen minimum disappears in tight
18 confinements because the decay of the mass flow rate due to the decreasing density effects is
19 overcome by the enhancing contribution to the flow provided by the fluid velocity slip at the
20 wall.

21 **Key words:** To be added during the online submission process (see [Keyword PDF](#)).

22 **1. Introduction**

23 Fluids confined within geometries of molecular dimensions are commonly encountered in
24 geological and biological systems (Bocquet & Charlaix 2010), as well as in many engineering
25 applications, e.g., membrane science (Mistry *et al.* 2021), that have been constantly growing
26 in recent years — fostered by the technological progress in the fabrication of nanofluidic
27 devices (Kavokine *et al.* 2021). In these flows, three significant length scales can be identified:
28 the diameter of fluid constituent particles σ , the flow characteristic length d , which is
29 related to the channel size, and the molecular mean free path (MFP) λ , which represents the
30 average distance travelled by particles between two consecutive collisions. The interplay of
31 phenomena occurring at these scales leads to complex fluid behaviour. Indeed, the continuum
32 approach based on the Navier-Stokes equations breaks down with increasing rarefaction
33 ($\lambda \sim d$), since the local thermodynamic equilibrium condition is not fulfilled. Likewise,

† Email address for correspondence: livio.gibelli@ed.ac.uk

34 the standard kinetic theory description is no longer accurate at the nanoscale where dense
 35 ($\lambda \sim \sigma$) and confinement ($d \sim \sigma$) effects come into play, implying that the Boltzmann
 36 equation must be replaced by more complicated kinetic models, such as the Enskog equation
 37 (Kremer 2010).

38 Despite the availability of computational procedures to describe the flow of confined fluids,
 39 the fundamental understanding of many phenomena occurring under tight confinement is
 40 still lacking. A notable example is that, for simple fluids, the Poiseuille mass flow rate (MFR)
 41 is found to monotonically increase in channels of molecular dimensions when the fluid
 42 density decreases, by using numerical solutions of the Enskog equation (Wu *et al.* 2016)
 43 and event-driven molecular dynamics simulations (Sheng *et al.* 2020). This behaviour is in
 44 sharp contrast with the long-standing recognition of flow mechanics in microchannels, which
 45 instead exhibits a non-monotonic variation of the MFR and the formation of a stationary
 46 point referred to as the “Knudsen minimum” (Cercignani & Sernagiotto 1966), as long as
 47 the channel is sufficiently long and does not contain any bends (Ho *et al.* 2020).

48 A possible explanation of the Knudsen minimum disappearance is that the transport in
 49 dense fluids changes from convection to molecular diffusion under tight confinements.
 50 Here, *molecular diffusion* is referred to as the diffusive mechanism which is driven by the
 51 interactions between fluid particles in the continuum limit ($\lambda \ll d$), and it is distinguished
 52 from the *Knudsen diffusion* that takes place in the free molecular limit ($\lambda \gg d$), where
 53 particles only collide ballistically with the wall (Xiao & Wei 1992). The dominance of
 54 diffusive transport at the nanoscale is known to take place for long alkanes in porous media,
 55 where the hydrodynamic description breaks down, although doubt remains for single-site gas
 56 molecules (Falk *et al.* 2015). Despite there is no unequivocal evidence that this behaviour also
 57 occurs for non-tortuous channels, some hints supporting the diffusive nature of Poiseuille
 58 flow transport in tight geometries are provided by the analysis of velocity profiles. These
 59 are no longer parabolic as expected for force/pressure-driven flows, but show a plug-like
 60 behaviour instead, suggesting the predominance of diffusive mechanisms (Firouzi & Wilcox
 61 2013). However, a conclusive proof regarding a crossover from convection to molecular
 62 diffusion in these systems, that is triggered by the fluid confinement, has still not been given.

63 The aim of this work is to perform a detailed investigation of the Knudsen minimum
 64 disappearance in straight nanochannels, and elucidate the underpinning physical reasons.
 65 There are two main findings. First, despite the molecular-like confinements, we show that
 66 diffusion does not dominate transport, and so the convective flow contribution cannot be
 67 neglected outside the free molecular regime. Second, we show that the monotonic increase
 68 of MFR can be attributed to the larger relative importance of the velocity slip at the wall,
 69 compared to the other physical mechanisms that are normal contenders at the microscale. The
 70 rest of the paper is organised as follows. In section 2 we outline the simulation approach used
 71 to numerically study the transport process. In section 3.1 we show that the Knudsen minimum
 72 vanishing in straight nanochannels cannot be attributed to diffusive processes, whereas in
 73 section 3.2 we prove that the contribution of the fluid slippage at the confining solid surface
 74 provides a satisfactory explanation of this recently discovered feature. A summary of the
 75 main results and conclusions follow in section 4.

76 2. Methodology

77 We consider force-driven Poiseuille flows inside a long tubular geometry with diameter d ,
 78 where the fluid is modelled using a system composed of hard-sphere particles with molecular
 79 diameter σ . The wall is assumed to be a structureless cylindrical surface and the fluid-wall
 80 interactions are described by the Maxwell scattering kernel with full tangential momentum
 81 accommodation coefficient, where impinging particles are diffusely reflected after being

82 thermalised with the wall. The exact time evolution of the monatomic hard-sphere system is
 83 simulated using event-driven molecular dynamics (EDMD). In these simulations, the state of
 84 the system jumps from one time to another corresponding to the upcoming collision through
 85 three basic steps: (a) evaluating the time of the earliest collision event, (b) moving ballistically
 86 all particles for that time interval, and (c) updating the velocity of the particles that have
 87 collided with another particle or the wall, according to elastic hard-sphere dynamics or the
 88 Maxwell scattering kernel, respectively. Note that the time step is not constant throughout
 89 the simulation run, like in regular MD simulations, as it depends on the spatial coordinates
 90 and velocities of all molecules in the system. More information on the simulation setup can
 91 be found in [Corral-Casas *et al.* \(2021\)](#).

92 Three dimensionless groups can be identified to systematically describe the different
 93 transport processes that may take place in this system, namely the reduced density, the
 94 confinement ratio, and the Knudsen number. The reduced density $\eta = n\pi\sigma^3/6$, where n is the
 95 number density, represents the number of fluid particles in the theoretical volume occupied by
 96 one hard-sphere. This first dimensionless group allows to differentiate between dense (large
 97 η values) and rarefied (low η values) gas flows. The confinement ratio $R = d/\sigma$ provides
 98 information about the degree of fluid inhomogeneity that arises because of the presence
 99 of walls, where tight confinements (low R values) are associated with a more prominent
 100 molecular layering next to the confining surface and, therefore, with an increase of the
 101 collision frequency of fluid particles with the wall. Finally, the Knudsen number $Kn = \lambda/d$
 102 quantifies the departure of the fluid from its local quasi-equilibrium case. The continuum
 103 approach can be used for $Kn \lesssim 0.01$, while non-equilibrium effects come progressively into
 104 play in the following three regimes: slip ($0.01 < Kn \lesssim 0.1$, where the continuum model still
 105 holds but different boundary conditions are needed to capture the “slippage” of fluid particles
 106 at the solid surface), transition ($0.1 < Kn \lesssim 10$, where the continuum description breaks
 107 down and kinetic equations must be used instead), and free molecular ($Kn > 10$, where
 108 molecules move ballistically between collisions with the confining wall). The expression of
 109 the MFP, derived from kinetic theory, is given by ([Kremer 2010](#))

$$110 \quad \lambda = \frac{16}{5\pi} \frac{\mu}{P} \sqrt{\frac{\pi kT}{2m}}, \quad (2.1)$$

111 where m is the molecular mass and P is the pressure, related to the density through $P = nkTZ$,
 112 in which k is the Boltzmann constant, T the temperature of the system, and Z is the fluid
 113 compressibility factor that can be accurately approximated by the equation of state for the
 114 hard-sphere fluid proposed in [Carnahan & Starling \(1969\)](#)

$$115 \quad Z = \frac{P}{nkT} = \frac{1 + \eta + \eta^2 - \eta^3}{(1 - \eta)^3}. \quad (2.2)$$

116 According to the Enskog theory, the shear viscosity μ of a hard-sphere fluid is given by

$$117 \quad \mu = \frac{5}{16\sigma^2} \sqrt{\frac{mkT}{\pi}} \mu_f = \frac{5}{16\sigma^2} \sqrt{\frac{mkT}{\pi}} \frac{1}{\chi} \left[1 + \frac{16}{5} \eta \chi + \frac{64}{25} \left(1 + \frac{12}{\pi} \right) \eta^2 \chi^2 \right], \quad (2.3)$$

118 where μ_f is the dense gas correction for the viscosity of a rarefied gas, and χ represents the
 119 contact value of the pair correlation function in a hard-sphere fluid in uniform equilibrium,
 120 which from the aforementioned equation of state reads

$$121 \quad \chi = \frac{1}{nb} \left(\frac{P}{nkT} - 1 \right) = \frac{1}{2} \frac{2 - \eta}{(1 - \eta)^3}, \quad (2.4)$$

122 where $b = 2\pi\sigma^3/3$ is the second virial coefficient ([Kremer 2010](#)).

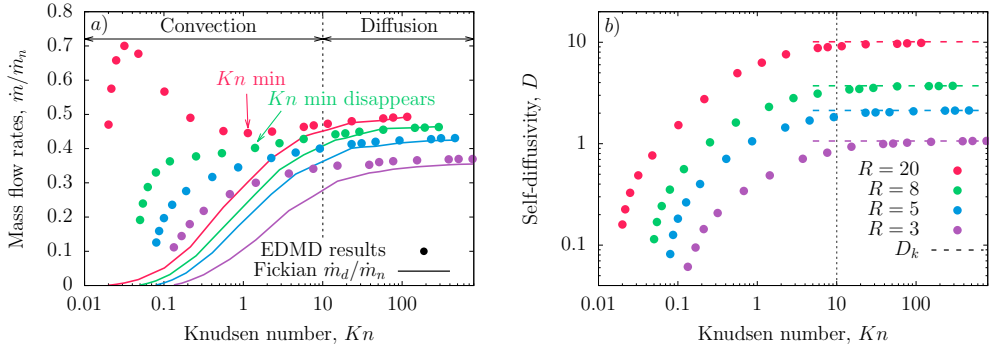


Figure 1: (a) Comparison between the dimensionless MFR provided by non-equilibrium simulations (symbols) and the theoretical predictions assuming Fickian diffusion, as given by Eq. (3.1) (lines). There is good agreement in the free molecular regime ($Kn \geq 10$), whilst Fick's law underestimates MFR elsewhere, which imply that convective transport terms cannot be neglected at any confinement. (b) Dependence of the self-diffusivity D on the Knudsen number Kn and the confinement ratio R . Dashed horizontal lines represent the theoretical value of the Knudsen self-diffusivity from Eq. (3.2) for each confinement ratio.

123 3. Results and discussion

124 3.1. Knudsen minimum disappearance: analysis based on diffusion

125 The Knudsen minimum disappearance, which was initially presented for the slit geometry
 126 in Wu *et al.* (2016), is demonstrated for a cylindrical pipe in this work, where it is seen
 127 to occur between $R = 20$ and $R = 8$ in figure 1(a). Here, we show transport results
 128 from non-equilibrium EDMD simulations that are performed in the presence of an external
 129 unidirectional force F along the axis of the channel, whose value is assumed to be sufficiently
 130 low so that the flow remains in the linear response regime — the artificial addition of heat
 131 is adequately dissipated by the wall. The numerical evaluation of the MFR for each case,
 132 depending on η and R , is obtained from a spatial integration of local densities and velocities.

133 As mentioned in section 1, the Knudsen minimum vanishing might be explained by
 134 supposing that, under molecular confinements, a crossover from convective to diffusive
 135 transport takes place up to the late transition regime ($Kn \lesssim 10$). This hypothesis is tested
 136 by comparing the actual MFR with the analytical estimate assuming that the transport is
 137 solely driven by diffusion, which is based on the Fick's first law where the MFR of diffusing
 138 particles \dot{m}_d follows a linear response with the density gradient along the axial z -direction
 139 dn/dz

$$140 \quad \dot{m}_d = -\frac{\pi d^2}{4} m D \frac{dn}{dz} = -\frac{D \pi d^2 m}{4kT \left(Z + \eta \frac{dz}{d\eta} \right)} \frac{dP}{dz}, \quad (3.1)$$

141 in which D is the self-diffusion coefficient. Note that the number density n and pressure P
 142 are interconnected using Eq. (2.2), with the pressure gradient being identified with the force
 143 F through the fundamental relation given by $-dP/dz = nF$.

144 However, before comparing the MFR simulation results with the predictions given by
 145 Eq. (3.1), self-diffusion results D are needed as this information is unavailable in the literature
 146 for the cylindrical geometry. Therefore, a set of equilibrium EDMD simulations is carried out,
 147 see details in Corral-Casas *et al.* (2021), where the self-diffusion coefficients are determined
 148 by means of the Einstein relation in the entire range of flow regimes, for different confinement
 149 ratios of interest. These simulation results are shown in figure 1(b), where it can be seen that,
 150 from a qualitative standpoint, self-diffusivities increase with Knudsen number because the

151 MFP becomes larger and therefore particles have more mobility before colliding with another
 152 entity in the system. At the same time, self-diffusivities increase with the flow characteristic
 153 length for a given Kn , as large R values imply less collisions with the diffuse wall model that
 154 hinder the molecular displacement in the streamwise direction. Note that in the free molecular
 155 limit, where there are just diffuse collisions with the wall, numerical results perfectly agree
 156 with the analytical Knudsen self-diffusivity prediction from kinetic theory (Xiao & Wei
 157 1992)

$$158 \quad D_k = \frac{2d}{3} \sqrt{\frac{2kT}{\pi m}}. \quad (3.2)$$

159 As presented in figure 1(a), it is found that the Fick's first law unsurprisingly reproduces
 160 the MFR simulation results very well in the free molecular regime. The slight disagreement
 161 in the tightest of confinements (for $R = 3$) can be attributed to the transition from Fickian
 162 to anomalous diffusion (e.g., of single-file type) as particles cannot overtake each other
 163 when moving along the channel. However, it is evident that Eq. (3.1) underestimates the
 164 mass transport along the remaining flow regimes ($Kn \lesssim 10$), and therefore the governing
 165 mechanism in this range of Kn is no longer purely diffusive. This clearly proves that, in straight
 166 channels, the supposed crossover from convection to diffusion does not occur even under
 167 tight confinements and, consequently, cannot explain the Knudsen minimum disappearance.
 168 Note that these results do not imply that diffusion is not the governing transport mechanism
 169 within more complex geometries, such as in microporous media, which will need to be
 170 addressed separately.

171 3.2. Knudsen minimum disappearance: analysis based on slip

172 As discussed so far, there are a number of mechanisms that influence the MFR through a
 173 channel, and so the best explanation for describing the features of the MFR dynamics can
 174 be inferred in the limits of the continuum ($Kn \approx 0$) and free molecular ($Kn \sim \infty$) regimes,
 175 as we illustrate in figure 2. As suggested by the analysis from section 3.1, the fluid flow is
 176 convective in nature in the continuum regime, regardless of R . When moving towards the
 177 free molecular regime (i.e., decreasing density values), the MFR initially increases as the
 178 viscosity decreases, implying that the fluid velocity arising as a response to a given external
 179 driving force will be larger. By contrast, the fluid flow is driven by Knudsen diffusion in the
 180 free molecular regime. This means that, when moving back towards the continuum regime
 181 (i.e., increasing density values), the MFR decreases as the molecular MFP shortens, implying
 182 lower self-diffusivities as observed in figure 1(b).

183 Under a sufficiently loose confinement ($R \gtrsim 60$ as shown in Appendix A), the Knudsen
 184 minimum existence follows from these two limiting behaviours. The MFR in the continuum
 185 regime is always larger than that in the free molecular regime and, therefore, the MFR curve
 186 must show two stationary points as depicted by the orange curve in figure 2, namely the
 187 Knudsen maximum and the Knudsen minimum. If the confinement is tighter, the continuum
 188 MFR is lower than the free molecular one. Accordingly, the flow transport curve may either
 189 form two stationary points, given by the blue dotted line, or else could show a monotonic
 190 increase throughout the entire range of Knudsen numbers, as represented by the blue solid
 191 line. It is then clear that, for the confined case, a necessary and sufficient condition for the
 192 Knudsen minimum to appear is that the Knudsen maximum shows up as well. Therefore,
 193 proving the disappearance of the Knudsen minimum is equivalent to demonstrating the
 194 Knudsen maximum vanishing. The latter question is easier to address as this local maximum
 195 falls in the continuum/slip regime ($Kn \lesssim 0.1$), where it can be tackled analytically using the
 196 Navier-Stokes equations with the first-order velocity slip boundary condition, which in its
 197 dimensionless form (a step-by-step derivation of this mathematical expression is presented

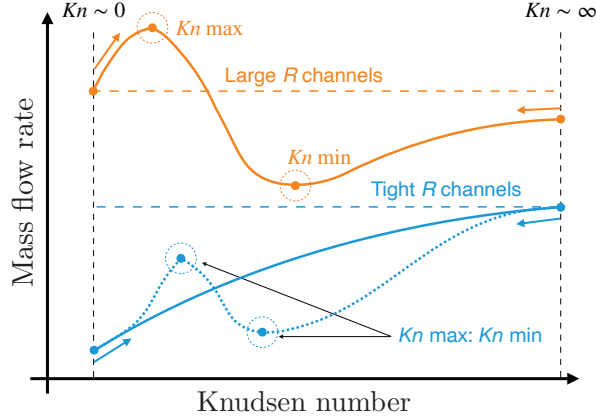


Figure 2: Qualitative analysis of the dimensionless MFR curves against the Knudsen number. Due to the governing transport mechanisms in the limiting flow regimes, the MFR will always increase/decrease when decreasing/increasing density in the continuum/free molecular regime. In sufficiently *large* channels (orange colour), where the continuum transport is larger than the free molecular one, the MFR curve must develop two stationary points as a response. On the other hand, for tighter confinements (blue colour) where the free molecular flow is larger than the continuum one, the MFR curve could either show the two stationary points or follow a monotonic increase instead, where the Knudsen minimum disappears.

198 in Appendix A) reads

$$199 \quad \dot{m} = \frac{\dot{m}_h}{\dot{m}_n} = \frac{3R\eta}{5\sqrt{\pi}\mu_f} (1 + 8\alpha Kn). \quad (3.3)$$

200 Note that two simplifying assumptions have been implicitly made. First, the slip coefficient
 201 α is assumed to be constant and equal to that of a rarefied gas, albeit slip phenomena are
 202 known to be more complicated when dealing with liquid-like densities (Martini *et al.* 2008;
 203 Hadjiconstantinou 2021). The validity of this assumption will be discussed later. Second, the
 204 velocity slip boundary condition at the wall is based on the strain rate and not on the stress
 205 tensor, leading to less accurate results if the wall is not at rest (Lockerby *et al.* 2004).

206 Eq. (3.3) clearly shows that there are three physical terms contributing to the MFR, namely
 207 the viscosity (i.e., via μ_f), the density (i.e., via η), and the slip (i.e., via $1 + 8\alpha Kn$). These
 208 terms vary with the reduced density but, for the following analysis, we find it more convenient
 209 to study the MFR with respect to the reduced specific volume $\nu = 1/\eta$, as in this way there is
 210 a one-to-one direct correspondence between ν and Kn . It should be stressed that this choice
 211 does not limit the generality of the conclusions. The relative importance of these terms can
 212 be singled out by evaluating their corresponding partial rates of change

$$213 \quad \frac{d\dot{m}}{d\nu} = \frac{d\eta}{d\nu} \left(\frac{\partial \dot{m}}{\partial \mu_f} \frac{d\mu_f}{d\eta} + \frac{\partial \dot{m}}{\partial \eta} + \frac{\partial \dot{m}}{\partial Kn} \frac{dKn}{d\eta} \right) = \frac{1}{\nu^2} (Q_\mu + Q_\eta + Q_\alpha), \quad (3.4)$$

214 where

$$215 \quad Q_\mu = \frac{3R\eta (1 + 8\alpha Kn)}{5\sqrt{\pi}\mu_f^2} \frac{d\mu_f}{d\eta}, \quad (3.5)$$

$$216 \quad Q_\eta = -\frac{3R(1 + 8\alpha Kn)}{5\sqrt{\pi}\mu_f}, \quad (3.6)$$

$$217 \quad Q_\alpha = \frac{24R\eta\alpha}{5\sqrt{\pi}\mu_f} \frac{dKn}{d\eta}. \quad (3.7)$$

218

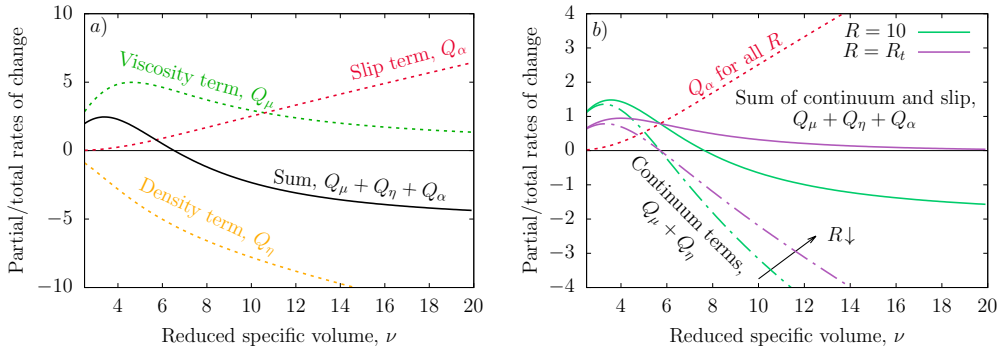


Figure 3: (a) Partial rates of change against the reduced specific volume, for $R = 20$, under the continuum framework of fluid modelling, which capture how flow transport is affected by a change of each of the underlying contributions. (b) Interplay between the continuum (dash-dotted) and the slip (dotted) contributions for different R values. For sufficiently large R values, the continuum contribution dominates and the sum of all rates of change (solid) crosses the x -axis, i.e., the Knudsen maximum appears. However, for tight channels, the continuum contribution is less relevant whereas slip remains the same, driving the overall rate of change to be positive throughout the entire range of ν values, with the Knudsen maximum disappearing as a consequence.

219 These individual contributions are presented in figure 3(a) for $R = 20$, in a range of ν
 220 values corresponding to $Kn \lesssim 0.1$, namely the slip regime. Here, the plot of Eq. (3.5) shows
 221 that the partial derivative of the MFR with respect to the viscosity, Q_μ , is always positive with
 222 increasing reduced specific volume. In particular, the rate of change is higher for low ν values,
 223 whereas its value decreases for large reduced specific volumes. Eq. (3.6) shows that the MFR
 224 partial derivative with respect to the density, Q_η , is always negative with increasing reduced
 225 specific volume. If the slip contribution is temporarily disregarded, the density is seen to
 226 become relevant over the viscosity at $\nu \approx 6$, and drives the MFR to decrease monotonically
 227 with further increase in the reduced specific volume. Eq. (3.7) shows that the MFR partial
 228 derivative with respect to the slip, Q_α , is always positive with increasing specific volume. In
 229 particular, the rate of change is almost negligible in the continuum regime while it becomes
 230 larger in the slip regime ($\nu \gtrsim 3.33$), where rarefaction effects become more prominent and
 231 the fluid slippage at the wall increasingly contributes to the overall MFR.

232 Three important observations are in order and presented in figure 3(b), that helped us to
 233 understand why the Knudsen minimum disappears only when confinements are tight. The
 234 first remark is that the viscosity and density contributions exactly counterbalance at the same
 235 ν regardless of R . This can be easily proved using Eqs. (3.5) and (3.6), and it is clearly shown
 236 by dashed lines, representing the sum of viscosity and density rates of change (dubbed the
 237 *continuum contribution* from here onwards), which always crosses the x -axis at $\nu = 5.711$.
 238 A second remark is that the magnitude of the rate of change of the continuum contribution
 239 reduces with tighter channels and so its absolute value decreases with lower R for a given ν
 240 value, as could also be deduced from Eqs. (3.5) and (3.6). The third remark is that the slip
 241 contribution (dotted line) is independent of R , as it is seen in Eq. (3.7), and so its relative
 242 importance grows when the confinement ratio reduces.

243 The interplay between the three aforementioned contributions (denoted by solid lines in
 244 figure 3(b), representing the sum of continuum and slip terms) significantly depends on the
 245 size of the channel, and we can mainly distinguish between two types of flow behaviours. For
 246 *large* channel sizes and starting from the continuum regime (low ν), the viscosity contribution
 247 initially dominates and leads the MFR to increase with ν . The region corresponding to low ν
 248 values can then be referred to as viscosity dominated since this contribution overcomes that

249 of density, and here the slip term is negligible. Unlike the viscosity term that gets weaker as
 250 the fluid rarefaction increases, the density term becomes progressively more important and
 251 causes the Knudsen maximum to form by eventually driving the MFR to decrease.

252 For tight confinements, viscosity is initially dominant and drives the MFR increase as
 253 in the previous case. However, now there is an interplay between density and slip in the
 254 region where the transport was previously density dominated, as the relative contribution
 255 of slip becomes more and more important for decreasing R . Indeed, as emphasised by the
 256 magnitude of the continuum and slip contributions in figure 3(b), there might be a threshold
 257 confinement ratio R at which the latter overcomes the former, preventing the formation of
 258 the expected Knudsen maximum. Therefore, the velocity slip at the boundary impels the
 259 MFR curve to monotonically increase throughout the entire range of flow regimes, with the
 260 Knudsen maximum (and so, the Knudsen minimum) disappearing as a consequence.

261 It is worth noticing that, within the simplified solution represented by Eq. (3.4), the
 262 Knudsen minimum disappearance can be determined by a simple argument. As the rate of
 263 change of the MFR is a continuous function that takes positive values in the continuum
 264 limit, a sufficient condition for the MFR to cross the x -axis could be defined by the Bolzano
 265 theorem

$$266 \quad \lim_{\nu \rightarrow \infty} (Q_\mu + Q_\eta + Q_\alpha) = \frac{8\sqrt{2}\alpha - 3R}{5\sqrt{\pi}} \leq 0. \quad (3.8)$$

267 Numerical evidence shows that this condition is not only sufficient but also necessary, and
 268 hence one may conclude that the threshold confinement ratio R_t for the Knudsen minimum
 269 disappearance is $R_t < 8\sqrt{2}\alpha/3$.

270 The analysis carried out in this section is based on two main simplifying considerations.
 271 The first assumption consists on using nominal values for density and viscosity in the Navier-
 272 Stokes equations, despite it is well-known that, under tight confinement, density is non-
 273 uniform across the channel and viscosity is no longer a local property of the position along
 274 the channel (Travis *et al.* 1997). However, there is a large body of evidence demonstrating that
 275 the hydrodynamic framework is valid down to nanoscale confinements (Bocquet & Charlaix
 276 2010), and our numerical simulations also showed an agreement (within 4.5% for $Kn \lesssim 0.01$)
 277 with the non-slip Hagen-Poiseuille solution, using nominal values of the fluid properties.
 278 The second assumption involves the use of a constant slip coefficient although, unlike the
 279 rarefied case, numerical evidence shows that it depends on the channel size, e.g., larger α
 280 with decreasing R values. However, the validity of the presented analysis is not undermined
 281 as the slip enhancement at lower R just results in the Knudsen minimum disappearance at a
 282 larger R_t , and therefore the results in figure 3(b) correspond to the worst case scenario.

283 4. Conclusions

284 We have studied the Knudsen minimum disappearance that occurs for Poiseuille flows in
 285 tight cylindrical geometries. High-fidelity EDMD simulations have been carried out in a wide
 286 range of reduced fluid densities η and channel confinement ratios R , in both equilibrium (to
 287 obtain the self-diffusivities needed in the Fickian framework) and non-equilibrium (directly
 288 evaluating the mass flow rate) setups. Although diffusion is supposed to be the main transport
 289 mechanism at the nanoscale, we found that the convective contribution to the mass flow rate
 290 cannot be disregarded — even under confinements of molecular dimensions. This convection-
 291 dominated transport, which is analytically studied using the Hagen-Poiseuille solution with
 292 first-order slip, is decoupled into its three fundamental contributions, namely viscosity,
 293 density, and slip. The individual influence of each of them on transport is assessed for different
 294 fluid rarefaction states and confinement ratios, which revealed that the disappearance of the

295 Knudsen minimum is a consequence of the interplay between these contributions. More
 296 specifically, the combined contribution of viscosity and density weakens in tight geometries,
 297 whereas the slip term remains the same when R decreases, and so its relative importance
 298 increases in this context. Therefore, the Knudsen minimum vanishing under tight confinement
 299 can be explained by the more accentuated importance of the fluid slippage at the wall. The
 300 relevance of this work underpins in its qualitative explanation of dense flow mechanisms
 301 at the molecular scale, which may help to better understand how slip, from a fundamental
 302 standpoint, affects the flow of dense gases/liquids confined within tight geometries, such as
 303 high-pressure methane transport in unconventional shale rocks or water transport in nano-
 304 structured filtration membranes.

305 **Funding.** This research was funded in whole, or in part, by the King Fahd University of Petroleum and
 306 Minerals (KFUPM), Saudi Arabia. M.K.B. and L.G. are funded by the Engineering and Physical Sciences
 307 Research Council (EPSRC) under grant numbers EP/V012002/1, EP/R007438/1. For the purpose of open
 308 access, the author has applied a CC BY public copyright licence to any Author Accepted Manuscript version
 309 arising from this submission.

310 **Declaration of interests.** The authors report no conflict of interest.

311 **Data availability statement.** The data that supports the findings of this study are openly available in
 312 Edinburgh DataShare repository at [http://doi.org/\[doi\]](http://doi.org/[doi]), reference number to be added during proofs' stage.

313 Appendix A.

314 The Navier-Stokes equations for the incompressible flow of a Newtonian fluid through an
 315 infinite cylindrical channel simplify to

$$316 \quad \frac{1}{r} \frac{d}{dr} \left(r \frac{du_z}{dr} \right) = \frac{1}{\mu} \frac{dP}{dz}, \quad (\text{A } 1)$$

317 where u_z is the fluid macroscopic velocity in the streamwise direction, and r is the radial
 318 direction. The first-order slip at the wall, $r = d/2$, can be written as

$$319 \quad u_s = -\alpha \lambda \left. \frac{du_z}{dr} \right|_{r=d/2}, \quad (\text{A } 2)$$

320 where u_s is the slip velocity, and $\alpha = 2/\sqrt{\pi}$ is the velocity slip coefficient (Gibelli 2012).
 321 The straightforward solution of the boundary value problem from Eqs. (A 1), (A 2) reads

$$322 \quad u_z(r) = \frac{1}{4\mu} \frac{dP}{dz} \left(r^2 - d\alpha\lambda - \frac{d^2}{4} \right). \quad (\text{A } 3)$$

323 The spatial integration of the velocity field over the cross section yields the Hagen-Poiseuille
 324 solution for the MFR

$$325 \quad \dot{m}_h = mn \int_0^{d/2} u_z(r) 2\pi r dr = -\frac{mn\pi d^4}{128\mu} \frac{dP}{dz} (1 + 8\alpha Kn). \quad (\text{A } 4)$$

326 Independently on the confinement ratio R , the MFR increases/decreases with the increas-
 327 ing/decreasing of the Knudsen number in the continuum/free molecular regimes (see
 328 discussion in the beginning of section 3.2). A sufficient condition for the Knudsen minimum
 329 to appear can be thus easily determined by imposing the MFR in the continuum regime to
 330 be larger than that in the free molecular regime. The dimensionless MFR in the continuum
 331 limit ($Kn \approx 0$) is given by Eq. (A 4) with $\alpha = 0$, i.e., the non-slip solution

$$332 \quad \frac{\dot{m}_h}{\dot{m}_n} = \frac{3R\eta_0}{5\sqrt{\pi}f_\mu}, \quad (\text{A } 5)$$

333 where it is assumed that the fluid is at its freezing point, corresponding to $\eta_0 = 0.494$
 334 for a fluid of hard-spheres (Sigurgeirsson & Heyes 2003). The normalising MFR here and
 335 elsewhere in the text, for instance explicitly in figures 1(a), 2, and Eq. (3.3), is

$$336 \quad \dot{m}_n = -mn_0 \frac{\pi d^2}{4} \frac{1}{m} \frac{1}{n_0} \frac{dP}{dz} \frac{d}{\sqrt{kT/m}} = -\frac{\pi d^3}{4\sqrt{kT/m}} \frac{dP}{dz}, \quad (\text{A } 6)$$

337 From the dimensionless MFR in the free molecular limit ($Kn \sim \infty$), provided by Eq. (3.1)
 338 with the Knudsen self-diffusivity from Eq. (3.2) as the proportionality factor and $Z = 1$ from
 339 Eq. (2.2)

$$340 \quad \frac{\dot{m}_d}{\dot{m}_n} = \frac{D_k}{d} \sqrt{\frac{m}{kT}} = \frac{2}{3} \sqrt{\frac{2}{\pi}}, \quad (\text{A } 7)$$

341 it is easily derived that the aforementioned (A5) \geq (A7) condition is always satisfied for
 342 $R \gtrsim 60$, represented by the orange curve in figure 2 depicting the behaviour in large channels.

REFERENCES

- 343 BOCQUET, L. & CHARLAIX, E. 2010 Nanofluidics, from bulk to interfaces. *Chemical Society Reviews* **39** (3),
 344 1073–1095.
- 345 CARNAHAN, N. F. & STARLING, K. E. 1969 Equation of state for nonattracting rigid spheres. *Journal of*
 346 *Chemical Physics* **51** (2), 635–636.
- 347 CERCIGNANI, C. & SERNAGIOTTO, F. 1966 Cylindrical poiseuille flow of a rarefied gas. *Physics Of Fluids*
 348 **9** (1), 40–44.
- 349 CORRAL-CASAS, C., GIBELLI, L., BORG, M. K., LI, J., AL-AFNAN, S.F.K. & ZHANG, Y. 2021 Self-diffusivity
 350 of dense confined fluids. *Physics of Fluids* **33** (8).
- 351 FALK, K., COASNE, B., PELLENO, R., ULM, F. J. & BOCQUET, L. 2015 Subcontinuum mass transport of
 352 condensed hydrocarbons in nanoporous media. *Nature Communications* **6**, 1–7.
- 353 FIROUZI, M. & WILCOX, J. 2013 Slippage and viscosity predictions in carbon micropores and their influence
 354 on CO₂ and CH₄ transport. *Journal of Chemical Physics* **138** (6).
- 355 GIBELLI, L. 2012 Velocity slip coefficients based on the hard-sphere Boltzmann equation. *Physics of Fluids*
 356 **24** (2).
- 357 HADJICONSTANTINO, N. G. 2021 An atomistic model for the Navier slip condition. *Journal of Fluid*
 358 *Mechanics* **912**, 1–13.
- 359 HO, M. T., LI, J., SU, W., WU, L., BORG, M. K., LI, Z. & ZHANG, Y. 2020 Rarefied flow separation in
 360 microchannel with bends. *Journal of Fluid Mechanics* **901**.
- 361 KAVOKINE, N., NETZ, R. R. & BOCQUET, L. 2021 Fluids at the Nanoscale: From Continuum to Subcontinuum
 362 Transport. *Annual Review of Fluid Mechanics* **53**, 377–410.
- 363 KREMER, G. M. 2010 *An Introduction to the Boltzmann Equation and Transport Processes in Gases*. Berlin,
 364 Heidelberg: Springer.
- 365 LOCKERBY, D. A., REESE, J. M., EMERSON, D. R. & BARBER, R. W. 2004 Velocity boundary condition at
 366 solid walls in rarefied gas calculations. *Physical Review E* **70** (1), 4.
- 367 MARTINI, A., ROXIN, A., SNURR, R. Q., WANG, Q. & LICHTER, S. 2008 Molecular mechanisms of liquid slip.
 368 *Journal of Fluid Mechanics* **600**, 257–269.
- 369 MISTRY, S., PILLAI, R., MATTIA, D. & BORG, M. K. 2021 Untangling the physics of water transport in boron
 370 nitride nanotubes. *Nanoscale* **13**, 18096–18102.
- 371 SHENG, Q., GIBELLI, L., LI, J., BORG, M. K. & ZHANG, Y. 2020 Dense gas flow simulations in ultra-tight
 372 confinement. *Physics of Fluids* **32** (9).
- 373 SIGURGEIRSSON, H. & HEYES, D. M. 2003 Transport coefficients of hard sphere fluids. *Molecular Physics*
 374 **101** (3), 469–482.
- 375 TRAVIS, K. P., TODD, B. D. & EVANS, D. J. 1997 Departure from Navier-Stokes hydrodynamics in confined
 376 liquids. *Physical Review E* **55** (4), 4288–4295.
- 377 WU, L., LIU, H., REESE, J. M. & ZHANG, Y. 2016 Non-equilibrium dynamics of dense gas under tight
 378 confinement. *Journal of Fluid Mechanics* **794**, 252–266.
- 379 XIAO, J. & WEI, J. 1992 Diffusion of Hydrocarbons Theory. *Chemical Engineering Science* **47**, 1123–1141.